Journal of Visualization, Vol. 8, No. 2 (2005) 85

Effect of Rim-Shroud Clearance on the Flow Developing around a Finite-Thickness Rotating Disk in a Cylindrical Enclosure

Watanabe, T. [1], Furukawa, H. [2] and Nakamura, I. [2]

1) EcoTopia Science Institute, Nagoya University, Furo, Chikusa, Nagoya 464-8603 Japan.

2) Faculty of Science and Technology, Meijo University, Shiogama, Tenpaku, Nagoya 468-8502 Japan.

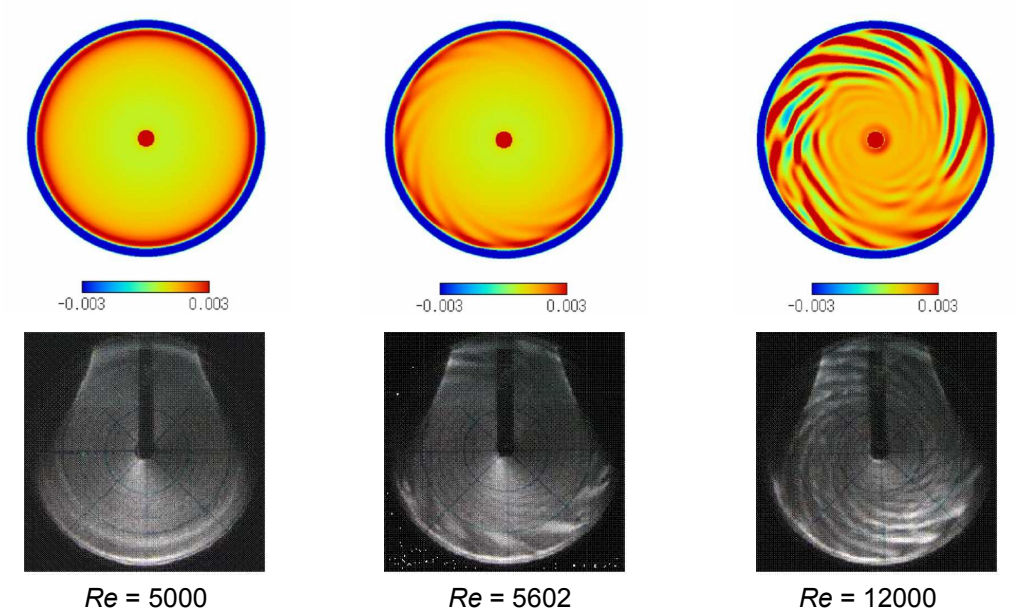

Re = 5000 *Re* = 5602 *Re* = 12000

Fig. 1. Numerical result of the axial velocity component profiles and experimental observation of flows in the Bödewadt layer. The ratios of radial clearance and upper and lower clearances to the inner radius of the enclosure are 0.106, 0.105 and 0.105, respectively.

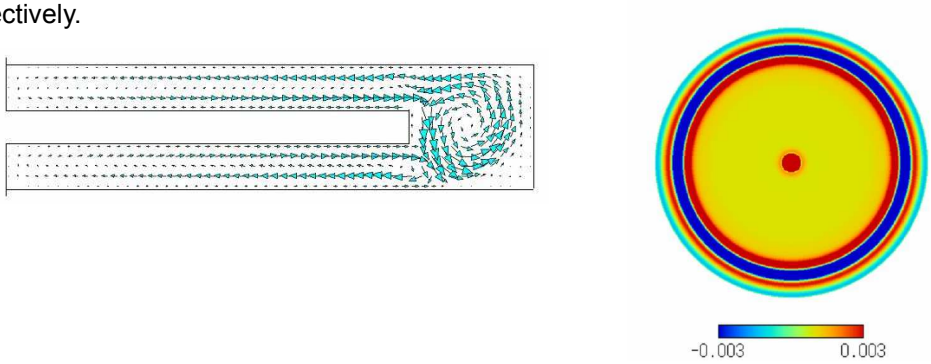

Fig. 2. Profile of the axial velocity component in the axial section and velocity vectors in the circumferential section at *Re* = 3000. The ratios of radial clearance and upper and lower clearances to the inner radius of the enclosure are 0.211, 0.070 and 0.070, respectively.

Numerical and experimental analysis is performed to examine flows around a rotating disk with finite thickness in a cylindrical enclosure. Figure 1 shows the flow patterns near the stationary end wall of enclosure. As the Reynolds number based on the circumferential velocity at the disk rim increases, the flows develop from those with circular rolls to turbulent spiral flows. The flow in Fig. 2 remains steady and it has a large vortex in the gap between the rotating disk and the shroud of the enclosure, while it is axisymmetric around the rotating axis. This result shows one of the evidences given by the complexity in nonlinear systems. The steady flow which is axisymmetric but is not symmetric in the axial direction has also been found in Taylor-Couette system with very small aspect ratio.

Direct Numerical Simulation of Gas-Solid Flow around a Circular Cylinder*

Liu, L.[1)] , Fan, J. R.[1)] , Ji, F.[1)] and Cen, K. F.[1)]

1) Institute of Thermal Power Engineering and CE&EE, Zhejiang University, Hangzhou 310027, Peoples' Republic of China.

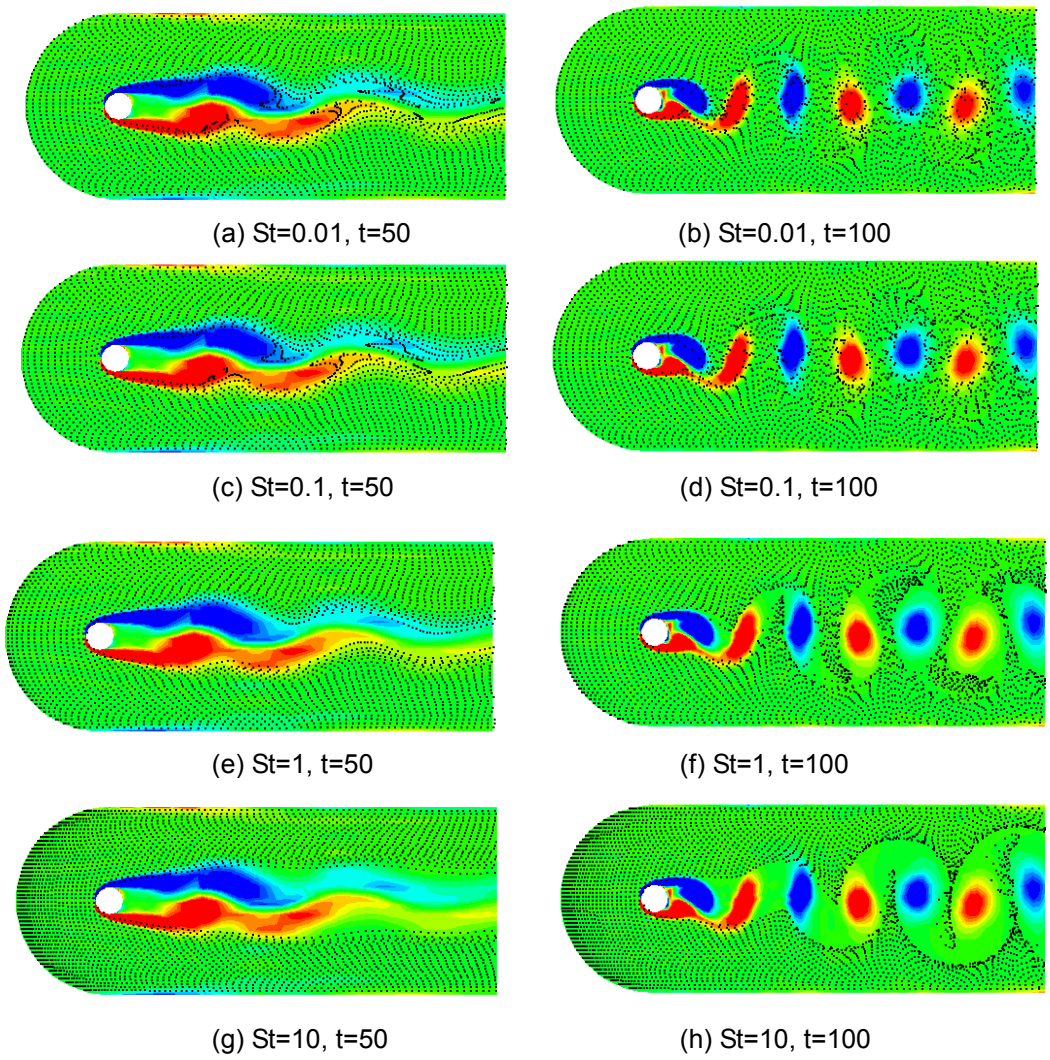

Fig. 1. Distribution of particles in the cylinder wake at *Re*=100.

0.

Figure. 1 shows the dispersion patterns of different Stokes number particles in a two-dimensional cylinder wake at *Re*=100. The gas structure is simulated by a spectral-element method with third-order accuracy and a Lagrangian approach is used to trace particle trajectory. The simulation results show that particle Stokes number is an important factor to characterize the particle dispersion in the cylinder wake. Smaller particles have more particle dispersion due to their well follow capability. They appear much similar dispersion trend as gas-phase vortex structure. With the Stokes numbers increasing, the particles are to be focused in the thin regions of vortex-scale boundaries and formed an organized structure.

*Supported by the National Natural Science Key Foundations of China (No. 50236030)

Journal of Visualization, Vol. 8, No. 2 (2005) 87

High Speed Differential Interferometry Used for Analyzing Aerooptic Aberrations

Desse, J. M.[1] and Bourez, J. P.[1]

1) Office National d'Etudes et de Recherches Aérospatiales, Centre de Lille, 5 Boulevard Paul Painlevé, 59045 LILLE Cedex, France. E-mail: Jean-Michel.Desse@onera.fr.

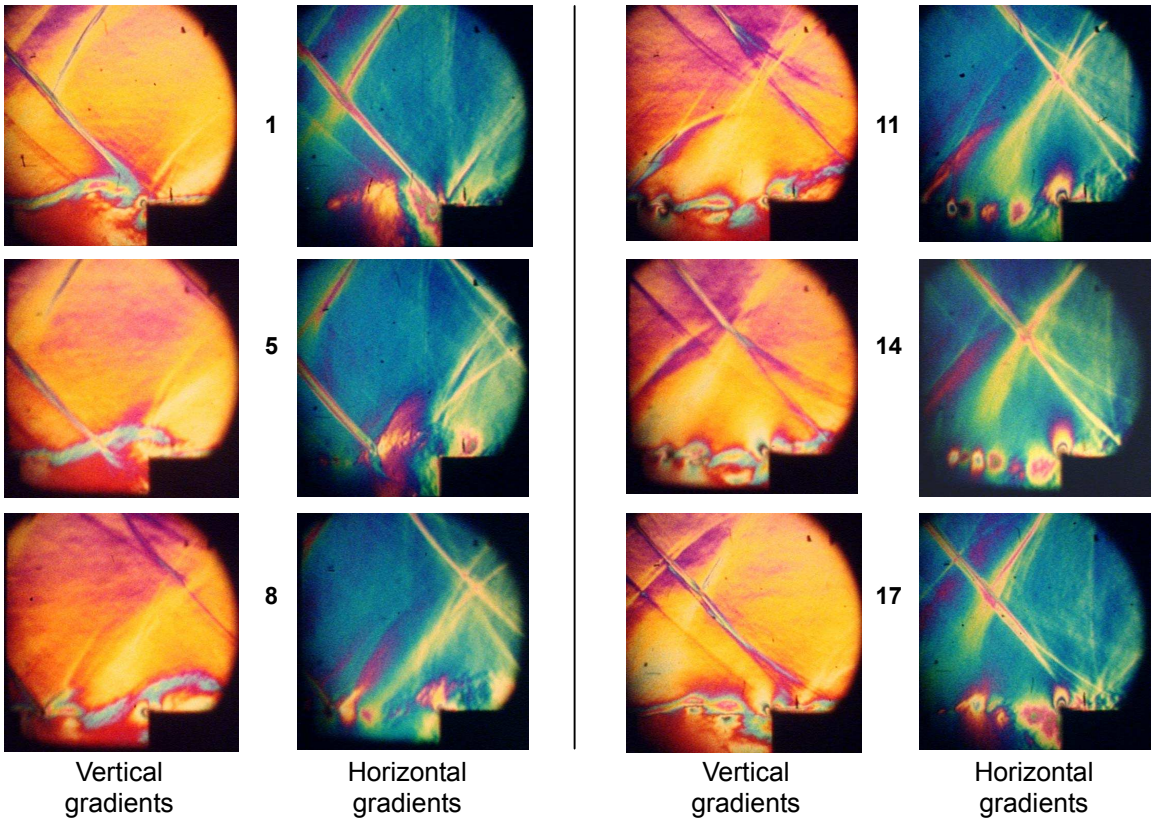

Fig. 1. High speed differential interferograms along the horizontal axis – ΔT = 28.5 μs – Mach 0.73.

High speed differential interferometry based on Wollaston prisms and polarized white light is used to analyze aerooptic aberrations induced by the flow above a cavity. The aim is both to propose an aerooptic statistical modeling validated by experiments and to constitute a full experimental data base, integrating aerodynamic data for the flow computation and optic aberrations data.

Two optical set ups have been defined to observe the gradients of refractive index of the flow along two perpendicular directions. Along the horizontal axis, high speed interferograms show the phenomenology of the coupling between the vortical structures of the mixing layer and the compression waves which move upstream the flow and are reflected by the upper floor of the test section. Figure 1 shows six high speed successive interferograms visualizing the horizontal and vertical gradients for a Mach number of 0.73. Each couple of interferograms is taken at the same phase of the pressure fluctuation and they cover one period of the phenomena. One see two different states of the mixing layer. On interferograms noted 1, 5 and 8, the interaction of the reflected waves with the mixing layer induce a disorganization of the vortices. On Interferograms 11, 14 and 17, one can clearly visualize the vortices in formation phase. However, these phenomena, observed with a confined flow configuration, are probably not representative of what should be observed in real flight conditions. Along the vertical axis, the analysis of interferograms has yielded the spatial distribution of the wavefront gradient and its evolution in time. A statistical analysis of the longitudinal and transverse refractive index gradients has been made from a sequence of 60 samples. These measurements have to be compared to measurements obtained with the Shack-Hartman technique.

Journal of Visualization, Vol. 8, No. 2 (2005) 88

Visualization of Soap Bubble Collapse with Acoustic Pressure Applied

Jaw, S. Y. [1]***, Chen, C. J.*** [2] ***and Hwang, R. R.*** [1]

1) Department of System Engineering and Naval Architecture, National Taiwan Ocean University, 2 Pei-Ning Road, Keelung, Taiwan, R.O.C.

2) College of Engineering, Florida A&M University-Florida State University, 2525 Pottsdamer Street, Tallahassee, Florida 32310-6064, U.S.A.

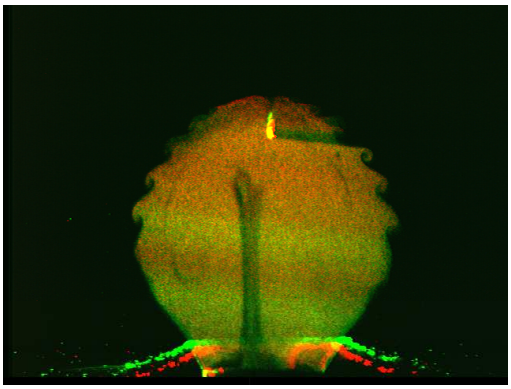

Fig. 1. Soap bubble is pierced to collapse.

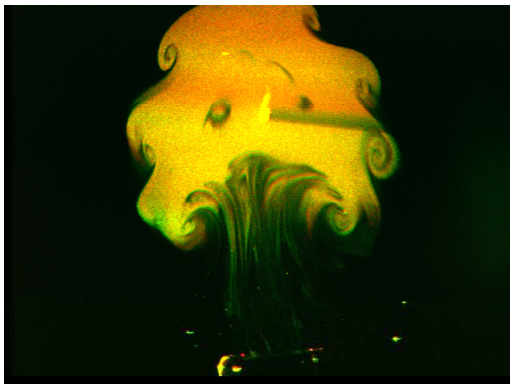

Fig. 2. An entrance jet is induced at the bottom.

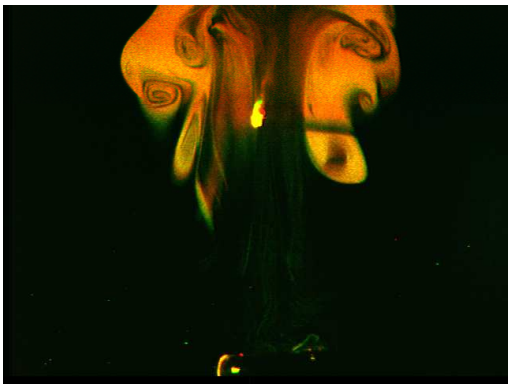

Fig. 3. Kelvin-Helmholtz vortex is formed.

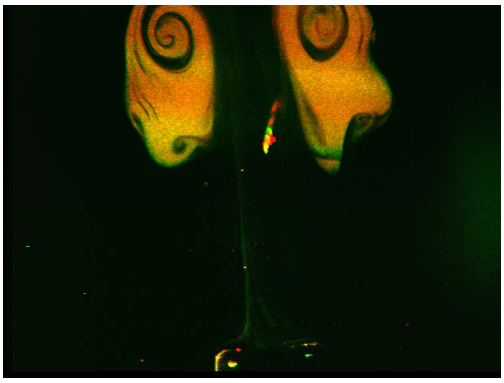

Fig. 4. Two separate vortices are formed.

A soap bubble, filled with smoke and sitting on a ring, is placed in an acoustic chamber with symmetric acoustic pressure applied on the two sides. A needle is used to pierce the bubble at the top. The soap bubble collapsed in such a way that the soap film is not in contact with the smoke, but "peeled away" from the smoke (Fig. 1).

When the bubble has fully collapsed, an entrance jet is induced at the bottom (Fig. 2). Kelvin-Helmholtz vortices are formed both inside and around the edge of the bubble (Fig. 3). Two separate vortices are formed as the entrance jet penetrates through the top of the bubble (Fig. 4).

.

Journal of Visualization, Vol. 8, No. 2 (2005) 89

Visualization of Mixing of Flow in Circular Tubes with Segmental Baffles

Al-Atabi, M. T. [1], Chin, S. B. [1] and Luo, X. Y. [2]

1) Mechanical Engineering Department, University of Sheffield, Sheffield S1 3JD, UK.

2) Department of Mathematics, University of Glasgow, University Gardens, Glasgow G12 8QW, UK.

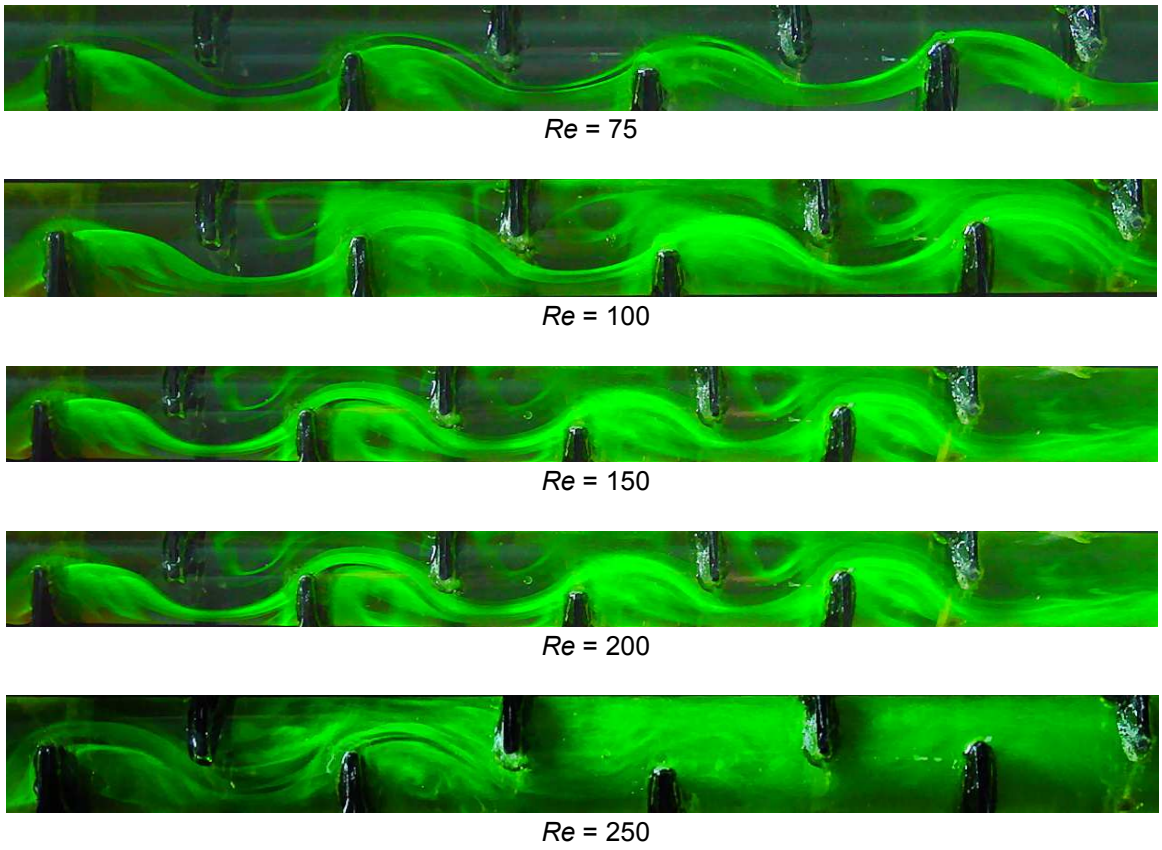

Fig. 1. Flow of water in a circular tube with segmental baffles. The flow is from left to right and the Reynolds numbers' values are based on the unobstructed tube diameter ($Re = \rho VD/\mu$).

Flow of liquids in circular tubes with segmental baffles is encountered in many fluid devices such as heat exchangers, mixers and biological flow models. Figure 1 above depicts laminar flow, visualized by Fluorescen dye, in a pipe (D = 21.5 mm) with eight equi-spaced semi-circular baffles. The baffles induce turbulence- like flow from Re_D>200 as evidenced by the enhanced mixing of the fluid downstream of the pipe.

Visualization of the Flow Pattern in the Rectangular Microchannel of a Miniature Heat Exchanger

Heinzel, V.[1)], Jianu, A.[1)] and Sauter, H.[1)]

1) Institute for Reactor Safety, Research Centre Karlsruhe, Postfach 3640, 76021 Karlsruhe, Germany.

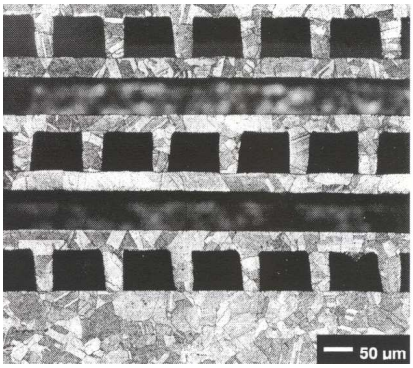

Fig. 1. Polished cross section of a diffusion-welded pile of elements forming a cross-flow heat exchanger element. Here: stainless steel.

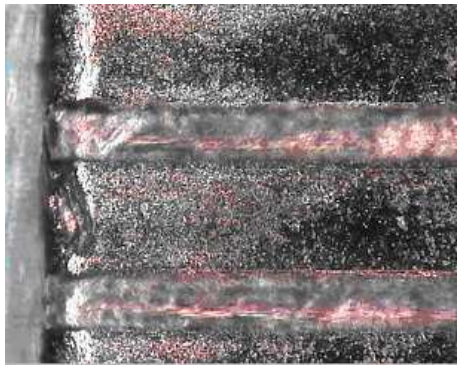

Fig. 2. Photo (top view) of a channel and the web walls (inlet on the left).

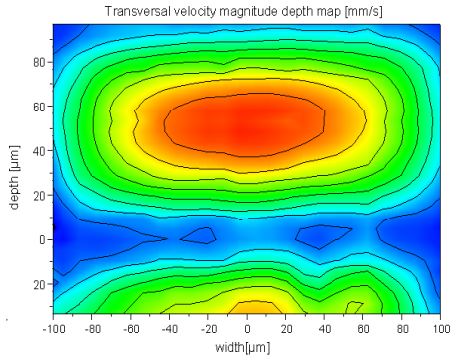

Fig. 3. Velocity map in a transversal plane of the plane of the channel (fully developed flow).

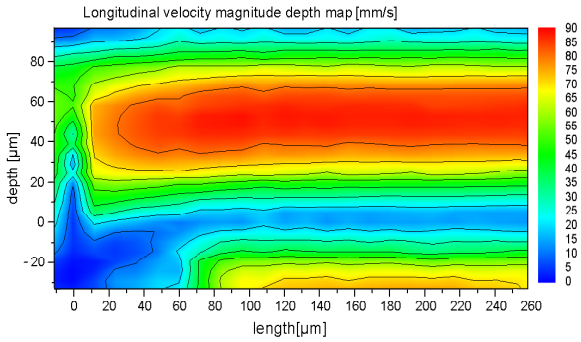

Fig. 4. Velocity map in the longitudinal middle channel (flow direction: left to right).

The cross-flow micro-channel heat exchangers are composed of slices, into which the channels are engraved by grinding ribbons. The rectangular channels have typical widths of 100 to 200 µm and a height of about the same dimensions. Web walls about 100 µm broad separate the channels. The slices are piled up and diffusion-welded to a heat exchanger segment (Fig. 1). Neighboring slices have orthogonally directed channels, therewith, creating the cross-flow heat exchanger.

The measurements reported here stem from the third generation of heat exchanger elements (copper made), presented in Fig. 2, which shows a photo (top view) of a channel and the web walls (inlet on the left); one may note the inlet dip and the near perfect mirror-like smoothness of the copper bottom at some distance from the cut inlet edge. The transition region from rough to smooth differs from one channel to the next.

The flow pattern in Fig. 3 gives the velocity field in a fully developed flow cross section. The flow was mapped throughout the channel depth experimentally, by acquiring PIV (particle image velocimetry) data in parallel planes approx. 5 µm apart. By re-plotting the data, it was transformed into depth velocity maps. The appearance of a mirrored velocity map, below the zero level, is induced by the near perfect mirror-like smoothness of the copper channel bottom (Fig. 2). As the images of the particles are mirrored, the measured velocity maps will show the effect alike, if measurement will be continued below the "zero" level.

Figure 4, which maps the velocity in the longitudinal middle plane of the channel, shows, from left to right: the inlet flow from the flat cell, the mechanical "dip" before the inlet, the onset of channel flow stabilization, the appearance of a mirror profile, below the zero level.